GEOLOGY | THE GEOLOGICAL SOCIETY OF AMERICA®

https://doi.org/10.1130/G46823.1

Manuscript received 26 April 2019
Revised manuscript received 30 July 2019
Manuscript accepted 6 August 2019

Published online 6 September 2019

The Ancestral Lhasa River: A Late Cretaceous trans-arc river that drained the proto–Tibetan Plateau

Andrew K. Laskowski[1], Devon A. Orme[1], Fulong Cai[2] and Lin Ding[2]
[1]Department of Earth Sciences, Montana State University, Bozeman, Montana 59717, USA
[2]Key Laboratory of Continental Collision and Plateau Uplift, Institute of Tibetan Plateau Research, Chinese Academy of Sciences, Beijing 100101, China

ABSTRACT

Late Cretaceous trench basin strata were deposited in the subduction zone that consumed Neo-Tethyan oceanic lithosphere along the southern margin of the proto–Tibetan Plateau. We conducted detrital zircon (DZ) U-Pb geochronology on six trench basin samples (n = 1716) collected near Dênggar, Tibet (~500 km west of Lhasa), to assess the provenance of these rocks and reconstruct Late Cretaceous sediment transport pathways. They contained DZ ages that point to a unique source around Lhasa city, north of the Late Cretaceous Gangdese magmatic arc. The modern Lhasa River catchment contains the requisite sources, and its main trunk transects the Gangdese magmatic arc, joining with the Yarlung River at a barbed junction at the India-Asia suture. We infer that the Lhasa River is an ancient feature that transported sediment to the subduction zone in Late Cretaceous time and persisted during India-Asia collision.

INTRODUCTION

Rivers that drain the eastern Tibetan Plateau flow along intercontinental suture zones: the Yarlung along the India-Lhasa terrane suture, the Salween (Nagqu) along the Lhasa-Qiangtang suture, the Mekong along the Sibumasu-Indochina suture, and the Yangtze along the Qiangtang–Songpan-Ganzi suture (e.g., Brookfield, 1998; Zhang et al., 2019). Despite reshaping and/or reorganization (Burrard and Hayden, 1907; Brookfield, 1998; Clark et al., 2004; Clift et al., 2006; Zhang et al., 2012; Zhang et al., 2019) during India-Asia collision (Yin and Harrison, 2000), the rivers remained pinned to the low-lying suture zones for millions of years. This is intuitive, because suture zones mark the locations of former trenches and persist as low-lying features during intercontinental collision (e.g., Fielding et al., 1994). The Lhasa River is an exception. Its headwaters originate in the eastern portion of the Lhasa terrane, the southernmost of the crustal fragments that comprised Eurasia prior to collision with India. Its main trunk drains to the southwest across the Gangdese Mountains to the location where it meets the east-flowing Yarlung River at an abrupt junction with the acute angle on the downstream side (Fig. 1). This so-called barbed junction, along with lack of evidence for structural control along the trans-Gangdese segment (Harrison et al., 1992) and the observation of antecedent tributaries (Shackleton and Chang, 1988), suggests that the Lhasa River was established prior to tectonic uplift. Despite these geomorphological observations, geological evidence for the hypothesized ancestral Lhasa River is lacking.

Prior to India-Asia collision, the southern Lhasa terrane was Andean-style (Murphy et al., 1997), comprising a Cretaceous to Paleocene subduction-accretion complex (e.g., Cai et al., 2012; Metcalf and Kapp, 2019) structurally overlying Jurassic and Cretaceous ophiolites (Göpel et al., 1984; McDermid et al., 2002; Hébert et al., 2012; Chan et al., 2015) and unconformably overlying Cretaceous to Paleocene Xigaze forearc basin strata (Einsele et al., 1994; Ding et al., 2005; Orme et al., 2015). These marginal assemblages are bounded to the north by the Late Triassic or Early Jurassic to Eocene Gangdese magmatic arc (Schärer et al., 1984; Lee et al., 2009; Zhu et al., 2011; Wang et al., 2016). Each feature developed in response to northward subduction of the Neo-Tethyan oceanic lithosphere beneath the southern Lhasa terrane as India converged on Eurasia (e.g., Shackleton, 1981; Tapponnier et al., 1981; Einsele et al., 1994; Cai et al., 2012; Orme and Laskowski, 2016; Metcalf and Kapp, 2017, 2019). Between 105 and 53 Ma, a retroarc fold-and-thrust belt developed in the central Lhasa terrane that accommodated >55% shortening, creating a relatively high-elevation mountain belt analogous to the modern Andes and Late Cretaceous North American Cordillera (Kapp et al., 2007; Leier et al., 2007). Contemporaneous sedimentary rocks are the primary record of the development of the convergent margin, including the growth of a forearc basin between ca. 110 and 51 Ma (An et al., 2014; Orme et al., 2015; Orme and Laskowski, 2016) and sedimentation in trench basins prior to ca. 85–70 Ma incorporation into the subduction-accretion complex (Cai et al., 2012; An et al., 2018; Wang et al., 2018; Metcalf and Kapp, 2019). Given that Lhasa terrane crystallization ages and isotopic compositions of igneous rocks (Zhu et al., 2011; Wang et al., 2016; Chapman and Kapp, 2017) and characteristic age spectra of sedimentary rocks (Gehrels et al., 2011) are well known, detrital zircon (DZ) geochronology is appropriate for determining sediment provenance. In addition, DZ geochronology enables comparison of Late Cretaceous sediment transport with that of the modern Tibetan Plateau. If Late Cretaceous sediment transport pathways are analogous to those of the modern drainages, then the simplest interpretation is that the pathway is long-lived, and the Late Cretaceous equivalent is antecedent.

We present data (n = 1716) from six DZ samples from Late Cretaceous (ca. 92–87 Ma) trench basin strata located near the town of Dênggar, ~500 km west of Lhasa city (Fig. 1). We also compiled DZ data (N = 6, n = 1662) from intact trench basin strata in the Lazi region, ~150 km to the east (Metcalf and Kapp, 2019). These data were compared with forearc basin strata to the north in the Saga (N = 18, n = 1577;

CITATION: Laskowski, A.K., Orme, D.A., Cai, F., and Ding, L., 2019, The Ancestral Lhasa River: A Late Cretaceous trans-arc river that drained the proto–Tibetan Plateau: Geology, v. 47, p. 1029–1033, https://doi.org/10.1130/G46823.1

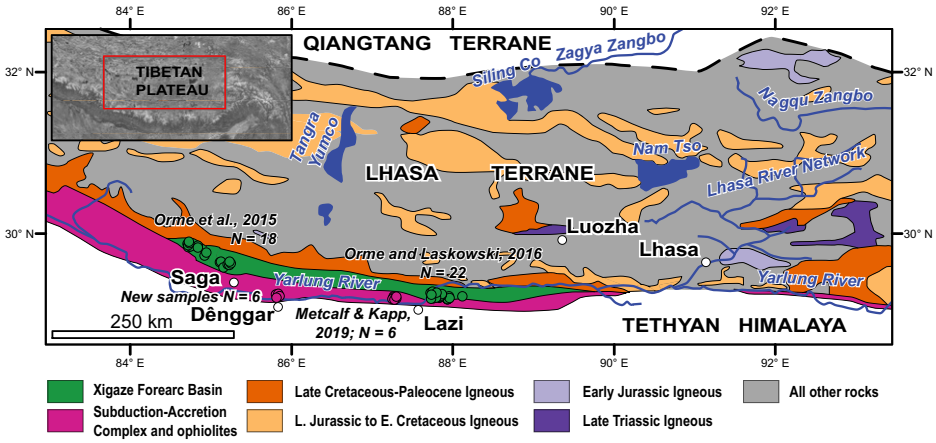

Figure 1. Tectonic map of the Lhasa terrane and Yarlung suture zone in south-central Tibet, modified from Zhu et al. (2011). Mesozoic and early Cenozoic igneous rocks of the Lhasa terrane are highlighted due to their importance for detrital zircon provenance analysis. Xigaze Group forearc basin sample locations are shown in green (Orme et al., 2015; Orme and Laskowski, 2016), whereas Rongmawa Formation (trench basin) samples are shown in pink (this study; Metcalf and Kapp, 2019). Major rivers and locations of towns were traced from the Esri World Topographic Map (http://arcg.is/0r4aaH).

Orme et al., 2015) and Lazi ($N = 22$, $n = 2164$; Orme and Laskowski, 2016) regions (Fig. 1). Our analysis reveals the distinct provenance of the trench basin and forearc basin strata, distinguished by the presence or absence of Late Triassic grains that were likely derived from the modern-day headwaters of the Lhasa River (Fig. 1). Based on these data, we infer that the trench basin is the ancient sedimentary record of the ancestral Lhasa River that transected the Late Cretaceous Gangdese magmatic arc and discharged into the Neo-Tethyan Ocean.

METHODS

Six samples were collected from fine- to medium-grained feldspatholithic sandstones interbedded with green and black shale, red siliceous shale, and chert. Samples were collected within a stratigraphic section beginning at the base (sample 62518DA1_0) and ending 962 m stratigraphically higher (sample 62518DA1_962). The stratigraphic log is included in the GSA Data Repository[1]. Our mapping indicates that the section is located within at least 1 km of intact stratigraphy between two moderately north-dipping faults that we interpret as splays of the Zhongba-Gyangze thrust (Burg and Chen, 1984). We correlate these strata to the Rongmawa Formation (Cai et al., 2012; Wang et al., 2018; Metcalf and Kapp, 2019) on the basis of similar lithologies and structural position.

DZ U-Pb ages were obtained for ~300 zircon grains per sample using a Photon Machines Analyte G2 excimer laser attached to a Thermo Element2 high-resolution, single-collector–inductively coupled plasma–mass spectrometer (HR-ICP-MS) at the Arizona LaserChron Center (University of Arizona, USA). Zircon targets were chosen randomly using the Crystal Site Selector program (creator: John H. Hartman, Department of Computer Science, University of Arizona, Tucson, Arizona, USA; jhh@cs.arizona.edu.). Hf isotopic data were obtained for all zircon grains with U-Pb ages younger than 300 Ma in the stratigraphically lowest and highest samples (n = 50) to isolate non-Gondwanan igneous rocks using an identical laser-ablation (LA) system attached to a Nu Plasma multicollector ICP-MS. Sample information and all analytical data are reported in Tables DR1–DR3 in the Data Repository. Analysis and data reduction followed the methods of Gehrels and Pecha (2014) and Pullen et al. (2018).

Kernel density estimate (KDE; Fig. 2) and multidimensional scaling (MDS; Fig. 3; Vermeesch, 2013) plots were generated using detritalPy (Sharman et al., 2018). Maximum depositional ages (MDAs) were calculated using three techniques: (1) age of the youngest single grain (YSG), (2) weighted mean age of the youngest two grains that overlapped at 1σ [YC1σ(2+)], and (3) weighted mean age of the youngest three grains that overlapped at 2σ ([YC2σ(3+)]; Table DR3). Source spectra (Fig. 2) were deconvolved using optimized nonnegative matrix factorization (NMF; Saylor et al., 2019), which uses an inverse approach to determine the optimum number of sources, reconstruct source spectra, and calculate weighting functions (Fig. 2). Provenance analysis was conducted by comparing trench basin DZ age distributions to the synthetic sources deconvolved from all trench basin samples using weighting functions (Fig. 2). Results from MDA and NMF calculations are reported in Tables DR4 and DR5.

RESULTS

The DZ age spectra from trench basin strata in the Dênggar region are remarkably internally consistent (Fig. 2). Furthermore, they are similar to trench basin samples near Lazi (Fig. 1), as evidenced by their proximity on the MDS plot (Fig. 3) and qualitative comparison of KDEs (Fig. 2). Both sample sets are characterized by prominent age-probability peaks at ca. 90 Ma, 120–130 Ma, 200–220 Ma, 500–550 Ma, and ca. 1200 Ma (Fig. 2). Lazi region samples have a higher relative abundance of ca. 90 Ma ages compared to Dênggar samples (Fig. 3). Forearc basin samples generally plot far from the trench basin samples on the MDS plot (Fig. 3), with separations between the Saga region and Lazi region samples (Figs. 1 and 2). We interpret these differences to preclude dominant reworking of forearc basin strata into the trench basin. A subset of Xigaze Group samples (N = 10) plots close to the trench basin samples (Fig. 3). These samples were divided by geographic location and combined to construct composite KDEs (group A, Fig. 2). The remaining samples comprise the composite KDEs labeled "group B" (N = 30). Group A samples display similar age-probability peaks and relative abundance to the trench basin samples, whereas group B is dominated by Early to middle Cretaceous ages (Fig. 2).

For the stratigraphically lowest sample, the YC1σ(2+) and the YC2σ(3+) MDAs are identical at 92.2 ± 0.65 Ma (mean square of weighted deviates [MSWD] = 0.71). There was good agreement among the YSG, YC1σ(2+), and YC2σ(3+) techniques in the second-highest sample (62518DA1_787), with MDAs of 86.9 ± 1.26 Ma, 87.1 ± 0.86 Ma, (MSWD = 0.06), and 88.7 ± 0.65 Ma (MSWD = 3.88), respectively. MDAs from the highest sample (62518DA1_962) were not robust. Therefore, we interpret that the Dênggar trench basin rocks were deposited between 92 and 87 Ma, similar to ca. 85 Ma MDAs for trench basin strata ~100 km to the west of Dênggar (Wang et al., 2018) and 90–85 Ma MDAs from the Lazi region samples (Figs. 1 and 3), but older than 73–71 Ma YSG MDAs from trench basin samples ~200 km to the east of Dênggar (Cai et al., 2012).

Hf isotopic data from the lowest and highest samples ranged from −15 to 14 ε_{Hf} (Fig. 4). Analyses for U-Pb ages between 220 and 200 Ma were between −12 and 4 ε_{Hf}. Two 190–180 Ma analyses were more positive at 7 and 14. Ages between 140 and 80 Ma displayed an increasingly positive trend from −14 to 13.

[1]GSA Data Repository item 2019363, sample information, LA-ICP-MS U-Pb data, LA-ICP-MS Hf data, maximum depositional age calculations, nonnegative matrix factorization results, and the measured stratigraphic section containing the samples, is available online at http://www.geosociety.org/datarepository/2019/, or on request from editing@geosociety.org.

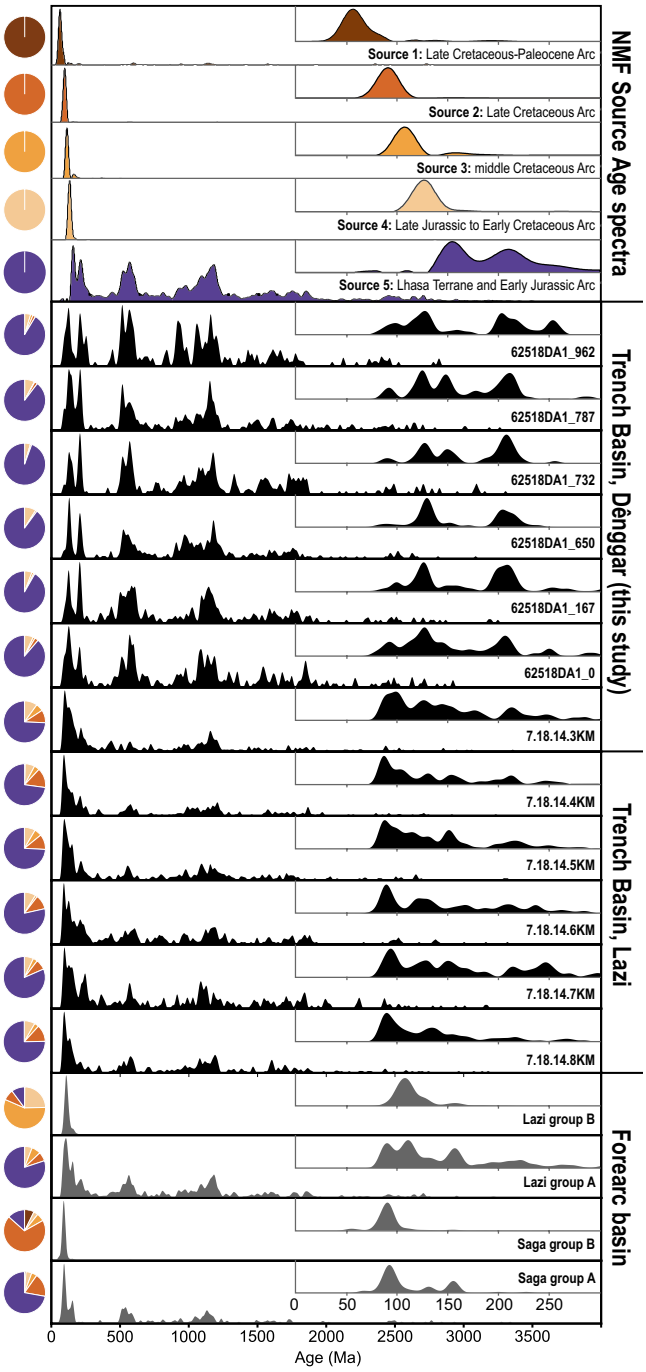

Figure 2. Non-normalized kernel density estimate (KDE) plots of individual Rongmawa Formation (southern Tibet) samples (black); composite KDEs of Xigaze Group forearc basin samples (gray) separated by geographic region (Fig. 1) and proximity to trench basin samples on MDS plot (Fig. 3); KDE representations of five optimal sources for all Rongmawa Formation and Xigaze Group forearc samples deconvolved using detrital zircon nonnegative matrix factorization (NMF; at top); and pie diagrams showing proportion of each NMF source in each age spectrum (at left, keyed by color). Spectra are plotted with relative probability on vertical axis, and U-Pb age between 0 and 4000 Ma on horizontal axis. Inset plot shows component of spectra between 0 and 300 Ma.

Nonnegative matrix factorization produced five optimal sources. Sources 1–4 (Fig. 2) are characterized by unimodal age-probability peaks ranging in age from Late Cretaceous–Paleocene to Late Jurassic–Early Cretaceous. Source 5 is more complicated, with age-probability peaks of Early Jurassic and Triassic age and additional, older peaks that mimic the trench basin samples (Fig. 2). Weighting functions, displayed as pie diagrams (Fig. 2), indicate that source 5 was the dominant source for trench basin samples and group A forearc basin samples (Fig. 2). In contrast, source 3 was dominant for Lazi group B samples, and source 2 was dominant for Saga group B samples.

DISCUSSION AND CONCLUSIONS

The similarities among our new DZ data, the Lazi region trench basin samples (Figs. 1–3), and other trench basin DZ data (Cai et al., 2012; Wang et al., 2018), all from the Rongmawa Formation, suggest common provenance. A different trench basin unit (Luogangcuo Formation) exposed near Saga (Fig. 1) was also deposited during Late Cretaceous time (88–81 Ma; An et al., 2018). It is distinguished based on its conglomeratic composition and DZ age spectra that largely lack the >170 Ma age-probability peaks (Fig. 2). However, samples from turbidites in the Luogangcuo Formation appear qualitatively similar to our samples (An et al., 2018), suggesting that the coarse facies are likely a marginal or isolated trench slope basin equivalent of the Rongmawa Formation derived from local sources. Based on these provenance similarities and Late Cretaceous MDAs for all trench basin samples, we interpret that they comprised an interrelated trench basin (Fig. 1).

The age-probability peaks that distinguish the trench basin samples from the majority of the forearc basin samples (group A) are represented by source 5 (Fig. 2). Source 5 age-probability peaks are readily explained by Early Jurassic igneous rocks (i.e., the Zedong arc southeast of Lhasa city), Triassic igneous rocks related to rifting of the Lhasa terrane from Australia (Zhu et al., 2011) or earliest Gangdese arc magmatism (Wang et al., 2018), and Paleozoic to Mesozoic strata of the Lhasa terrane (e.g., Leier et al., 2007; Gehrels et al., 2011). The 220–200 Ma age-probability peaks in the trench basin samples are rare in the forearc basin samples, except for minor occurrences in Lazi group A samples (8/10), all from the Upper Cretaceous Xigaze Group. Bedrock sources for 220–200 Ma ages are rare in the Lhasa terrane. Modern exposures are located to the northeast of Lhasa city, in the Luozha region, and in small exposures south of Lhasa city (Fig. 1; Wang et al., 2018). A compilation of Hf isotopic data from the Lhasa terrane (Zhu et al., 2011) revealed that sources with similar Hf compositions and U-Pb ages (220–200 Ma) only occur in the southern and central Lhasa terrane east of Luozha (Figs. 1 and 4). In contrast, the remaining Xigaze Group samples are dominated by Late Jurassic to Paleocene age-probability peaks that are readily explained by more widespread Late Jurassic to Paleocene igneous rocks of the Gangdese magmatic arc (Figs. 1 and 4).

Trench basin samples and Lazi forearc basin group A samples require a source region with Paleozoic and Mesozoic Lhasa terrane sedimentary rocks and Late Triassic to Early Jurassic igneous rocks (i.e., source 5; Fig. 2). Therefore, we interpret that the region surrounding Lhasa city (Fig. 1) is the most likely source. If correct, sediment must have dispersed across the Gangdese magmatic arc during Late Cretaceous time to reach the trench basin without significant dilution, largely bypassing the forearc basin. These criteria appear to require a broad catchment area in the central-eastern Lhasa terrane, a confined sediment transport pathway across the magmatic arc, and axial transport along the southern Lhasa terrane margin to at least as far west as Dênggar (Fig. 1). The modern Lhasa River fits the first two criteria: It has a large catchment area (32,800 km^2; Prasch et al., 2013) in the central-eastern Lhasa terrane that includes the rare Late Triassic exposures, and it flows to the southwest along a constricted fluvial valley (<5 km wide), transecting the Gangdese magmatic arc. It discharges into the Yarlung River,

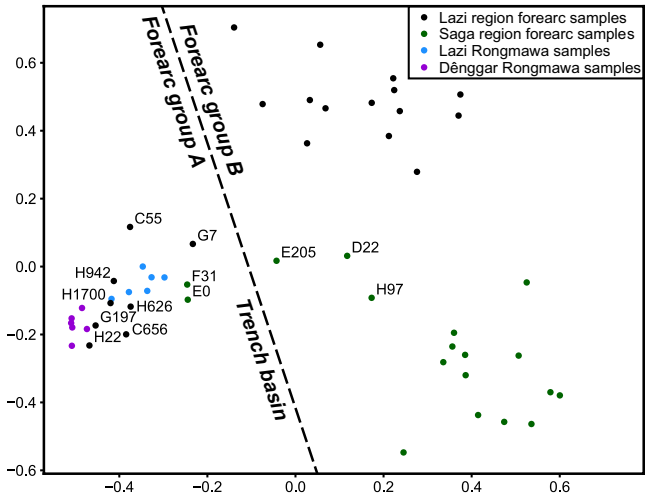

Figure 3. Multidimensional scaling (MDS; Vermeesch, 2013) results for all Xigaze Group forearc strata and Rongmawa Formation trench basin strata (southern Tibet), with interpreted boundary (dashed line) between samples displaying local Gangdese magmatic arc provenance and samples displaying distal, central Lhasa terrane provenance. Plot shows Kolmogorov-Smirnoff dissimilarities between samples as a map where similar samples cluster and differing samples plot far apart. Sample names are provided for select forearc samples from Orme et al. (2015) and Orme and Laskowski (2016) that plot close to Rongmawa Formation samples.

which flows along the southern Lhasa terrane parallel to the former trench. Based on the DZ provenance analysis, paired Hf isotopic data, the lack of evidence for structural control of the Lhasa River (Harrison et al., 1992), and the peculiar barbed junction with the Yarlung River, we interpret that the Lhasa River was antecedent to India-Asia collision. Our results support the linkages among surface uplift, enhanced erosion, and cooling that are implicit in interpreting thermochronology results along the Lhasa River (e.g., Harrison et al., 1992; Tremblay et al., 2015). The interpreted sediment transport pathway is analogous to the modern Fuji River in Japan, which transects magmatic arc highlands through a gorge west of Mount Fuji, discharges into the submarine Suruga Canyon, and connects to the >400-km-long, trench-parallel Nankai Deep Sea Channel carved by turbidity currents flowing axially along the Nankai Trough (e.g., Shimamura, 1989).

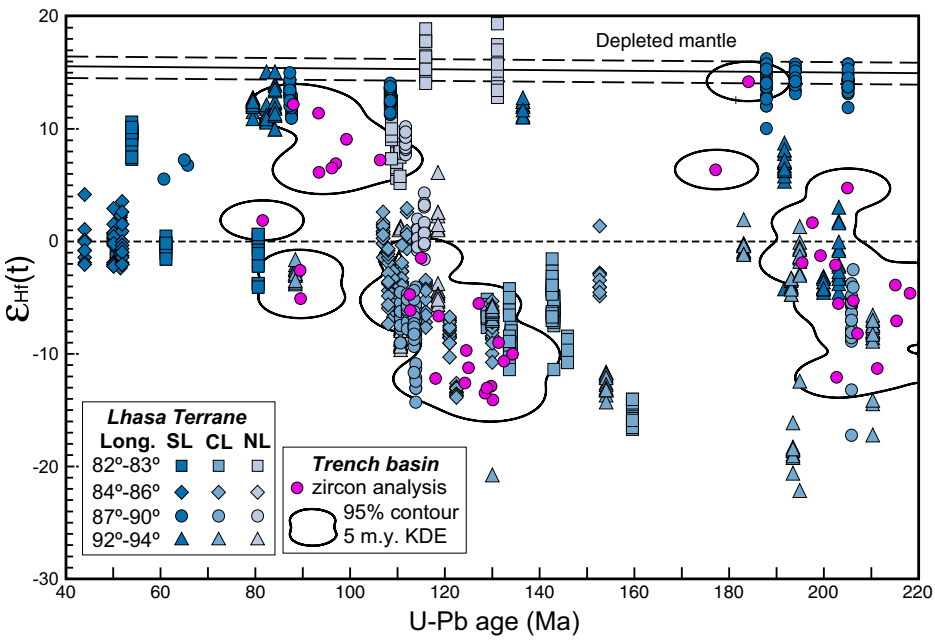

Figure 4. Paired detrital zircon Hf isotopic data and U-Pb ages from our Rongmawa Formation (southern Tibet) samples (n = 50; pink circles) plotted on Hf evolution diagram and compared against Lhasa terrane reference data from Zhu et al. (2011) (blue symbols); 95% contour is shown for three-dimensional (3-D) kernel density estimate (KDE) surface with 5 m.y. x-axis bandwidth and 1 ε_{Hf} y-axis bandwidth calculated from Rongmawa Formation data, created with HafniumPlotter (Sundell et al., 2019). Reference data are split into four longitudinal (Long.) swaths between 82°E and 94°E, shown by shades of blue, and by position within the Lhasa terrane, shown by different symbols. SL—southern Lhasa terrane; CL—central Lhasa terrane; NL—northern Lhasa terrane. Data were normalized to chondritic uniform reservoir (CHUR; dashed line at 0 ε_{Hf}). Depleted mantle isotopic composition is shown with 95% confidence intervals (solid line and long-dashed lines).

ACKNOWLEDGMENTS

We thank Institute of Tibetan Plateau Research personnel Guo Xudong for assistance with field work and Dr. Wang Chao for assistance with permitting. Financial support for this research was provided by the National Natural Science Foundation of China (grant 41490615 to Ding), by the U.S. National Science Foundation (grant EAR-1649254 to the Arizona LaserChron Center, University of Arizona), and by Montana State University. We thank the reviewers for their comments and Science Editor Chris Clark for handling.

REFERENCES CITED

An, W., Hu, X., Garzanti, E., BouDagher-Fadel, M.K., Wang, J., and Sun, G., 2014, Xigaze forearc basin revisited (south Tibet): Provenance changes and origin of the Xigaze ophiolite: Geological Society of America Bulletin, v. 126, p. 1595–1613, https://doi.org/10.1130/B31020.1.

An, W., Hu, X., and Garzanti, E., 2018, Discovery of Upper Cretaceous Neo-Tethyan trench deposits in south Tibet (Luogangcuo Formation): Lithosphere, v. 10, p. 446–459, https://doi.org/10.1130/L690.1.

Brookfield, M.E., 1998, The evolution of the great river systems of southern Asia during the Cenozoic India-Asia collision: Rivers draining southwards: Geomorphology, v. 22, p. 285–312, https://doi.org/10.1016/S0169-555X(97)00082-2.

Burg, J.P., and Chen, G.M., 1984, Tectonics and structural zonation of southern Tibet, China: Nature, v. 311, p. 219–223, https://doi.org/10.1038/311219a0.

Burrard, S.G., and Hayden, H.H., 1907, A Sketch of the Geography and Geology of the Himalaya Mountains and Tibet: Calcutta, India, Superintendent of Government Printing, 336 p.

Cai, F., Ding, L., Leary, R.J., Wang, H., Xu, Q., Zhang, L., and Yue, Y., 2012, Tectonostratigraphy and provenance of an accretionary complex within the Yarlung-Zangpo suture zone, southern Tibet: Insights into subduction-accretion processes in the Neo-Tethys: Tectonophysics, v. 574–575, p. 181–192, https://doi.org/10.1016/j.tecto.2012.08.016.

Chan, G.H.N., Aitchison, J.C., Crowley, Q.G., Horstwood, M.S.A., Searle, M.P., Parrish, R.R., and Chan, J.S.-L., 2015, U-Pb zircon ages for Yarlung Tsangpo suture zone ophiolites, southwestern Tibet, and their tectonic implications: Gondwana Research, v. 27, p. 719–732, https://doi.org/10.1016/j.gr.2013.06.016.

Chapman, J.B., and Kapp, P., 2017, Tibetan magmatism database: Geochemistry Geophysics Geosystems, v. 18, p. 4229–4234, https://doi.org/10.1002/2017GC007217.

Clark, M.K., Schoenbohm, L.M., Royden, L.H., Whipple, K.X., Burchfiel, B.C., Zhang, X., Tang, W., Wang, E., and Chen, L., 2004, Surface uplift, tectonics, and erosion of eastern Tibet from large-scale drainage patterns: Tectonics, v. 23, TC1006, https://doi.org/10.1029/2002TC001402.

Clift, P.D., Blusztajn, J., and Nguyen, A.D., 2006, Large-scale drainage capture and surface uplift in eastern Tibet–SW China before 24 Ma inferred from sediments of the Hanoi Basin, Vietnam: Geophysical Research Letters, v. 33, L19403, https://doi.org/10.1029/2006GL027772.

Ding, L., Kapp, P., and Wan, X., 2005, Paleocene–Eocene record of ophiolite obduction and initial India-Asia collision, south central Tibet: Tectonics, v. 24, TC3001, https://doi.org/10.1029/2004TC001729.

Einsele, G., Liu, B., Dürr, S., Frisch, W., Liu, G., Luterbacher, H.P., Ratschbacher, L., Ricken, W., Wendt, J., and Wetzel, A., 1994, The Xigaze forearc basin: Evolution and facies architecture (Cretaceous, Tibet): Sedimentary Geology, v. 90, p. 1–32, https://doi.org/10.1016/0037-0738(94)90014-0.

Fielding, E., Isacks, B., Barazangi, M., and Duncan, C., 1994, How flat is Tibet?: Geology, v. 22, p. 163–167, https://doi.org/10.1130/0091-7613(1994)022<0163:HFIT>2.3.CO;2.

Gehrels, G., and Pecha, M., 2014, Detrital zircon U-Pb geochronology and Hf isotope geochemistry of Paleozoic and Triassic passive margin strata of western North America: Geosphere, v. 10, p. 49–65, https://doi.org/10.1130/GES00889.1.

Gehrels, G., Kapp, P., DeCelles, P., Pullen, A., Blakey, R., Weislogel, A., Ding, L., Guynn, J., Martin, A., McQuarrie, N., and Yin, A., 2011, Detrital zircon geochronology of pre-Tertiary strata in the Tibetan-Himalayan orogen: Tectonics, v. 30, TC5016, https://doi.org/10.1029/2011TC002868.

Göpel, C., Allègre, C.J., and Xu, R.-H., 1984, Lead isotopic study of the Xigaze ophiolite (Tibet): The problem of the relationship between magmatites (gabbros, dolerites, lavas) and tectonites (harzburgites): Earth and Planetary Science Letters, v. 69, p. 301–310, https://doi.org/10.1016/0012-821X(84)90189-4.

Harrison, T.M., Copeland, P., Kidd, W., and Yin, A., 1992, Raising Tibet: Science, v. 255, p. 1663–1670, https://doi.org/10.1126/science.255.5052.1663.

Hébert, R., Bezard, R., Guilmette, C., Dostal, J., Wang, C.S., and Liu, Z.F., 2012, The Indus-Yarlung Zangbo ophiolites from Nanga Parbat to Namche Barwa syntaxes, southern Tibet: First synthesis of petrology, geochemistry, and geochronology with incidences on geodynamic reconstructions of Neo-Tethys: Gondwana Research, v. 22, p. 377–397, https://doi.org/10.1016/j.gr.2011.10.013.

Kapp, P., DeCelles, P.G., Leier, A.L., Fabijanic, J.M., and He, S., 2007, The Gangdese retroarc thrust belt revealed: GSA Today, v. 17, no. 7, p. 4–9, https://doi.org/10.1130/GSAT01707A.1.

Lee, H.-Y., Chung, S.-L., Lo, C.-H., Ji, J., Lee, T.-Y., Qian, Q., and Zhang, Q., 2009, Eocene Neotethyan slab breakoff in southern Tibet inferred from the Linzizong volcanic record: Tectonophysics, v. 477, p. 20–35, https://doi.org/10.1016/j.tecto.2009.02.031.

Leier, A.L., Kapp, P., Gehrels, G.E., and DeCelles, P.G., 2007, Detrital zircon geochronology of Carboniferous–Cretaceous strata in the Lhasa terrane, southern Tibet: Basin Research, v. 19, p. 361–378, https://doi.org/10.1111/j.1365-2117.2007.00330.x.

McDermid, I.R.C., Aitchison, J.C., Davis, A.M., Harrison, T.M., and Grove, M., 2002, The Zedong terrane: A Late Jurassic intra-oceanic magmatic arc within the Yarlung-Tsangpo suture zone, southeastern Tibet: Chemical Geology, v. 187, p. 267–277, https://doi.org/10.1016/S0009-2541(02)00040-2.

Metcalf, K., and Kapp, P., 2017, The Yarlung suture mélange, Lopu Range, southern Tibet: Provenance of sandstone blocks and transition from oceanic subduction to continental collision: Gondwana Research, v. 48, p. 15–33, https://doi.org/10.1016/j.gr.2017.03.002.

Metcalf, K., and Kapp, P., 2019, History of subduction erosion and accretion recorded in the Yarlung suture zone, southern Tibet, *in* Treloar, P.J., and Searle, M.P., eds., Himalayan Tectonics: A Modern Synthesis: Geological Society, London, Special Publications, v. 483, p. 12–38, https://doi.org/10.1144/SP483.12.

Murphy, M., Yin, A., Harrison, T., and Durr, S., 1997, Did the Indo-Asian collision alone create the Tibetan Plateau?: Geology, v. 25, p. 719–722, https://doi.org/10.1130/0091-7613(1997)025<0719:DTIACA>2.3.CO;2.

Orme, D.A., and Laskowski, A.K., 2016, Basin analysis of the Albian–Santonian Xigaze forearc, Lazi region, south-central Tibet: Journal of Sedimentary Research, v. 86, p. 894–913, https://doi.org/10.2110/jsr.2016.59.

Orme, D.A., Carrapa, B., and Kapp, P., 2015, Sedimentology, provenance and geochronology of the Upper Cretaceous–Lower Eocene western Xigaze forearc basin, southern Tibet: Basin Research, v. 27, p. 387–411, https://doi.org/10.1111/bre.12080.

Prasch, M., Mauser, W., and Weber, M., 2013, Quantifying present and future glacier melt-water contribution to runoff in a central Himalayan river basin: The Cryosphere, v. 7, p. 889–904, https://dx.doi.org/10.5194/tc-7-889-2013.

Pullen, A., Ibanez-Mejia, M., Gehrels, G., Giesler, D., and Pecha, M., 2018, Optimization of a laser ablation–single collector–inductively coupled plasma–mass spectrometer (Thermo Element 2) for accurate, precise, and efficient zircon U-Th-Pb geochronology: Geochemistry Geophysics Geosystems, v. 19, p. 3689–3705, https://doi.org/10.1029/2018GC007889.

Saylor, J.E., Sundell, K.E., and Sharman, G.R., 2019, Characterizing sediment sources by non-negative matrix factorization of detrital geochronological data: Earth and Planetary Science Letters, v. 512, p. 46–58, https://doi.org/10.1016/j.epsl.2019.01.044.

Schärer, U., Xu, R.-H., and Allègre, C.J., 1984, U-Pb geochronology of Gangdese (Transhimalaya) plutonism in the Lhasa-Xigaze region, Tibet: Earth and Planetary Science Letters, v. 69, p. 311–320, https://doi.org/10.1016/0012-821X(84)90190-0.

Shackleton, R.M., 1981, Structure of southern Tibet—Report on a traverse from Lhasa to Khatmandu organized by Academia-Sinica: Journal of Structural Geology, v. 3, p. 97–105, https://doi.org/10.1016/0191-8141(81)90060-2.

Shackleton, R.M., and Chang, C., 1988, Cenozoic uplift and deformation of the Tibetan Plateau: The geomorphological evidence: Philosophical Transactions of the Royal Society of London, ser. A, Mathematical and Physical Sciences, v. 327, p. 365–377, https://doi.org/10.1098/rsta.1988.0134.

Sharman, G.R., Sharman, J.P., and Sylvester, Z., 2018, detritalPy: A Python-based toolset for visualizing and analysing detrital geo-thermochronologic data: The Depositional Record, v. 4, p. 202–215, https://doi.org/10.1002/dep2.45.

Shimamura, K., 1989, Topography and sedimentary facies of the Nankai Deep Sea Channel, *in* Taira, A., and Masuda, F., eds., Sedimentary Facies in the Active Plate Margin: Tokyo, Japan, Terra Scientific Publishing Company, p. 529–556.

Sundell, K., et al., 2019, HafniumPlotter: https://github.com/kurtsundell/HafniumPlotter/commits/master/ (accessed March 2019).

Tapponnier, P., et al., 1981, The Tibetan side of the India-Eurasia collision: Nature, v. 294, p. 405–410, https://doi.org/10.1038/294405a0.

Tremblay, M.M., Fox, M., Schmidt, J.L., Tripathy-Lang, A., Wielicki, M.M., Harrison, T.M., Zeitler, P.K., and Shuster, D.L., 2015, Erosion in southern Tibet shut down at ~10 Ma due to enhanced rock uplift within the Himalaya: Proceedings of the National Academy of Sciences of the United States of America, v. 112, p. 12030–12035, https://doi.org/10.1073/pnas.1515652112.

Vermeesch, P., 2013, Multi-sample comparison of detrital age distributions: Chemical Geology, v. 341, p. 140–146, https://doi.org/10.1016/j.chemgeo.2013.01.010.

Wang, C., Ding, L., Zhang, L.-Y., Kapp, P., Pullen, A., and Yue, Y.-H., 2016, Petrogenesis of Middle-Late Triassic volcanic rocks from the Gangdese belt, southern Lhasa terrane: Implications for early subduction of Neo-Tethyan oceanic lithosphere: Lithos, v. 262, p. 320–333, https://doi.org/10.1016/j.lithos.2016.07.021.

Wang, H.-Q., Ding, L., Kapp, P., Cai, F.-L., Clinkscales, C., Xu, Q., Yue, Y.-H., Li, S., and Fan, S.-Q., 2018, Earliest Cretaceous accretion of Neo-Tethys oceanic subduction along the Yarlung Zangbo suture zone, Sangsang area, southern Tibet: Tectonophysics, v. 744, p. 373–389, https://doi.org/10.1016/j.tecto.2018.07.024.

Yin, A., and Harrison, T.M., 2000, Geologic evolution of the Himalayan-Tibetan orogen: Annual Review of Earth and Planetary Sciences, v. 28, p. 211–280, https://doi.org/10.1146/annurev.earth.28.1.211.

Zhang, J.Y., Yin, A., Liu, W.C., Wu, F.Y., Lin, D., and Grove, M., 2012, Coupled U-Pb dating and Hf isotopic analysis of detrital zircon of modern river sand from the Yalu River (Yarlung Tsangpo) drainage system in southern Tibet: Constraints on the transport processes and evolution of Himalayan rivers: Geological Society of America Bulletin, v. 124, p. 1449–1473, https://doi.org/10.1130/B30592.1.

Zhang, P., Najman, Y., Mei, L., Millar, I., Sobel, E., Carter, A., Barfod, D., Dhuime, B., Garzanti, E., Govin, G., Vezzoli, G., and Hu, X., 2019, Palaeodrainage evolution of the large rivers of East Asia, and Himalayan-Tibet tectonics: Earth-Science Reviews, v. 192, p. 1–107, https://doi.org/10.1016/j.earscirev.2019.02.003.

Zhu, D.-C., Zhao, Z.-D., Niu, Y., Mo, X.-X., Chung, S.-L., Hou, Z.-Q., Wang, L.-Q., and Wu, F.-Y., 2011, The Lhasa terrane: Record of a microcontinent and its histories of drift and growth: Earth and Planetary Science Letters, v. 301, p. 241–255, https://doi.org/10.1016/j.epsl.2010.11.005.

Printed in USA